ADVANCED MATERIALS
www.advmat.de

Realizing Over 13% Efficiency in Green-Solvent-Processed Nonfullerene Organic Solar Cells Enabled by 1,3,4-Thiadiazole-Based Wide-Bandgap Copolymers

Xiaopeng Xu, Ting Yu, Zhaozhao Bi, Wei Ma, Ying Li, and Qiang Peng**

Two novel wide-bandgap copolymers, PBDT-TDZ and PBDTS-TDZ, are developed based on 1,3,4-thiadiazole (TDZ) and benzo[1,2-b:4,5-b′]dithiophene (BDT) building blocks. These copolymers exhibit wide bandgaps over 2.07 eV and low-lying highest occupied molecular orbital (HOMO) levels below −5.35 eV, which match well with the typical low-bandgap acceptor of ITIC, resulting in a good complementary absorption from 300 to 900 nm and a low HOMO level offset (≤0.13 eV). Compared to PBDT-TDZ, PBDTS-TDZ with alkylthio side chains exhibits the stronger optical absorption, lower-lying HOMO level, and higher crystallinity. By using a single green solvent of *o*-xylene, PBDTS-TDZ:ITIC devices exhibit a large open-circuit voltage (V_{oc}) up to 1.10 eV and an extremely low energy loss (E_{loss}) of 0.48 eV. At the same time, the desirable high short-circuit current density (J_{sc}) of 17.78 mA cm^{-2} and fill factor of 65.4% are also obtained, giving rise to a high power conversion efficiency (PCE) of 12.80% without any additive and post-treatment. When adopting a homotandem device architecture, the PCE is further improved to 13.35% (certified as 13.19%) with a much larger V_{oc} of 2.13 V, which is the best value for any type of homotandem organic solar cells reported so far.

Organic solar cells (OSCs) have attracted considerable attention as a promising technology for clean and renewable energy conversion due to their advantages of low cost, light weight, and solution-processing ability for flexible and large-area devices.[1–3] Historically, fullerene derivatives dominated the field of acceptor materials for a long time in OSCs.[4,5] However, the inherent defects of fullerene derivatives blocked the commercialization progress of OSCs, such as costly synthetic and purification procedures, poor light harvesting ability in the visible region, difficult regulation of energy levels, and unstable morphology.[6,7] Therefore, nonfullerene alternatives have emerged recently to overcome the mentioned issues above.[8] Rapid progress has already been made in nonfullerene organic solar cells (NF-OSCs) during the past few years, which promoted the power conversion efficiencies (PCEs) exceeding 13% in both single-junction and tandem cells.[9,10]

In order to obtain high-performance NF-OSCs, complementary absorption of the active layer is perquisite, enabling to absorb sufficient sunlight and generate more excitons.[11] From the previous research work, fused ring-based small molecules with low bandgaps, such as 2,2′-((2Z,2′Z)-((5,5′-(4,4,9,9-tetrakis(4-hexylphenyl)-4,9-dihydro-s-indaceno[1,2-b:5,6-b′]dithiophene-2,7-diyl) bis(4-(2-ethylhexyl)thiophene-5,2-diyl)) bis(methanylylidene))-bis(3-oxo-2,3-dihydro-1H-indene-2,1-diylidene))dimalononitrile (IEIC),[12] 3,9-bis(2-methylene-(3-(1,1-dicyanomethylene)-indanone)-5,5,11,11-tetrakis(4-hexylphenyl)-dithieno[2,3-d:2′,3′-d′]-s-indaceno[1,2-b:5,6-b′]-dithiophene (ITIC),[13] 3,9-bis(2-methylene-(5&6-methyl-(3-(1,1-dicyanomethylene)-indanone)-5,5,11,11-tetrakis(4-hexylphenyl)-dithieno[2,3-d:2′,3′-d′]-s-indaceno[1,2-b:5,6-b′]-dithiophene (IT-M),[14] 3,9-bis(2-methylene-(5&6-fluoro-(3-(1,1-dicyanomethylene)-indanone)-5,5,11,11-tetrakis(4-hexylthienyl)-dithieno[2,3-d:2′,3′-d′]-s-indaceno[1,2-b:5,6-b′]-dithiophene (ITIC-Th1),[15] and 3,9-bis(2-methylene-(5,6-difluoro-(3-(1,1-dicyanomethylene)-indanone)-5,5,11,11-tetrakis(4-hexylphenyl)-dithieno[2,3-d:2′,3′-d′]-s-indaceno[1,2-b:5,6-b′]-dithiophene (IT-4F),[9] etc., might be the most successful type of nonfullerene acceptors in NF-OSCs, which showed good solubility, high crystallinity, favorable charge transport property, and strong optical absorption in the range of 600–800 nm.[16] Concerning the complementary absorption as mentioned above, excellent large bandgap polymer donors with strong absorption coefficients in the short wavelength range are highly desirable. On the other hand, the good energy level alignment between the used donor and acceptor materials should also be considered because it could significantly affect the related exciton dissociation and energy loss (E_{loss}).[16–18] Recent studies have shown that high-performance NF-OSCs could be realized with even much

Dr. X. P. Xu, T. Yu, Prof. Y. Li, Prof. Q. Peng
Key Laboratory of Green Chemistry and Technology
of Ministry of Education
College of Chemistry
and State Key Laboratory of Polymer Materials Engineering
Sichuan University
Chengdu 610064, P. R. China
E-mail: qiangpengjohnny@yahoo.com
Z. Z. Bi, Prof. W. Ma
State Key Laboratory for Mechanical Behavior of Materials
Xi'an Jiaotong University
Xi'an 710049, P. R. China
E-mail: msewma@mail.xjtu.edu.cn
The ORCID identification number(s) for the author(s) of this article can be found under https://doi.org/10.1002/adma.201703973.

DOI: 10.1002/adma.201703973

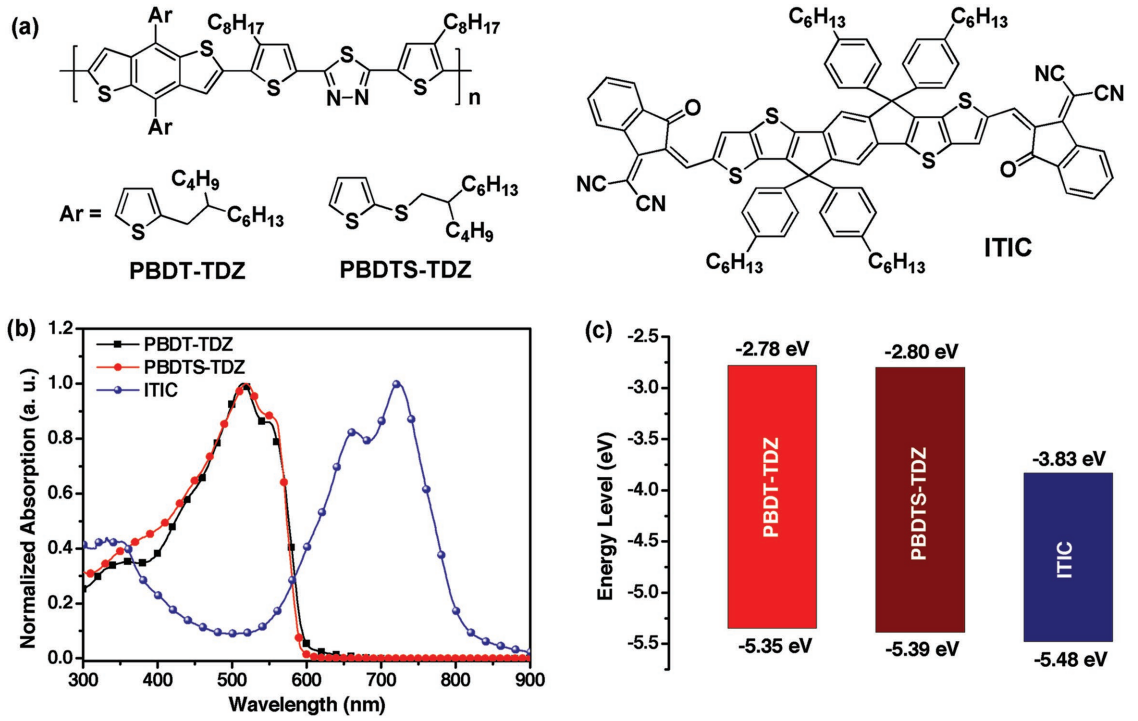

Figure 1. a) Chemical structures of the copolymers and ITIC. b) Normalized absorption of the copolymer and ITIC films. c) Energy level diagram of the copolymers and ITIC.

smaller E_{loss} values compared to the fullerene-based counterparts.[16–18] Therefore, developing excellent wide-bandgap polymeric donors is still a charming topic for further improving the device performance of NF-OSCs.

Apart from the material design, meticulous morphology control and sophisticated device engineering also play the important roles in elevating the efficiency of OSCs.[19] Many useful strategies have been applied to finely control the morphology by choosing appropriate solvents and additives as well as using hot spin-coating technology or post-treatments, such as thermal annealing and solvent vapor annealing.[17,20–23] However, in most cases, halogenated solvents (e.g., chlorobenzene (CB), 1,2-dichlorobenzene (DCB), chloroform (CF), etc.) and halogenated additives (e.g., 1,8-diiodoctane, 1-chloronaphthalene, etc.) are often adopted, which are harmful to human health and the environment.[24] The hot spin-coating process and tedious post-treatments, on the other side, inevitably suffer from the reproducibility issues, which are not practically accessible for mass printable production in the future.[25] Thus, it is still a great challenge for achieving highly efficient OSCs by just using a single but environment-friendly solvent without any post-treatment. Certainly, the tradeoff between the optical absorption and film thickness should also be balanced. The typical thickness of active layers (≈100 nm) is insufficient for harvesting enough photons due to the limited absorption ability.[26] Therefore, homotandem solar cells stacked with two sub-cells containing the same active layer in series would be a good choice to break such limitation and improving the device performance further.[26–28]

Herein, we design and synthesize two novel wide-bandgap copolymers based on 1,3,4-thiadiazole (TDZ) and benzo[1,2-b:4,5-b′]dithiophene (BDT), PBDT-TDZ and PBDTS-TDZ (**Figure 1**), for fabricating highly efficient NF-OSCs. Thiadiazole cycles have been widely studied in pharmaceutical chemistry due to their remarkably broad spectrum of biological activities.[29–32] As one of the thiadiazole isomers, TDZ associates with conjugated *p* and *π* electrons as well as distinct regions of positive and negative charges.[29] TDZ cycle is highly polarizable with a large electron affinity, which can be used as an excellent electron acceptor block for constructing high-performance D–A copolymers in the OSCs. However, TDZ-based copolymer donors received less attention and showed unsatisfactory device performances.[33–38] On the other hand, BDT unit features a weak electron-donating property, which is a good candidate as the donor block for building wide-bandgap copolymers. In addition, BDT unit possesses the rigid and large coplanar structure for inducing an improved *π*–*π* stacking of their D–A conjugated copolymers.[3] Therefore, we first demonstrate here the successful copolymer donors based on TDZ-BDT for efficient NF-OSCs. As expected, these two copolymers exhibited a wide bandgap over 2.07 eV (comparable to that of P3HT: 2.0 eV), which could match well with the typical low-bandgap acceptor of ITIC, thus giving rise to a complementary absorption in the range of 300–800 nm. The resulting copolymers also had the low-lying highest occupied molecular orbital (HOMO) levels (below −5.35 eV), leading to a small HOMO offset (≤0.13 eV) when blended with ITIC. If using a halogen-free solvent of *o*-xylene, a large open-circuit voltage (V_{oc}) of 1.10 eV and an extremely low E_{loss} of 0.48 eV could be obtained from PBDTS-TDZ:ITIC devices. Such high V_{oc} and low E_{loss} did not sacrifice the short-circuit current density (J_{sc}) (17.78 mA cm^{-2}) and fill factor (FF) (65.4%), thus giving rise to a PCE of 12.80%. It must

be noted that this high PCE value is facile to be realized by just using a single green solvent without any post-treatment, which can simplify the device fabrication for further applications, such as tandem devices. Finally, by employing a homotandem device structure, the PCE was further improved to 13.35% (certified as 13.19%) with a high V_{oc} of 2.13 V, which is the best value for homotandem NF-OSCs reported so far.

The synthetic routes of the monomers and the copolymers are shown in Scheme S1 (Supporting Information). Detailed synthesis and purification procedures as well as structure characterizations are provided in the Supporting Information. These two copolymers showed a good solubility in common solvents, such as tetrahydrofuran (THF), CF, CB, DCB, etc. The number average molecular weights (M_ns) were 31.6 and 35.9 kDa, and the polydispersity indices were 2.1 and 1.9 for PBDT-TDZ and PBDTS-TDZ, respectively, estimated by gel permeation chromatography. The decomposition temperatures (T_d, 5% weight loss) were determined to be 407 and 338 °C for PBDT-TDZ and PBDTS-TDZ, showing their good thermal stabilities (Figure S1, Supporting Information). No obvious endothermal and exothermal peaks were observed from room temperature up to 300 °C (Figure S1b, Supporting Information), which was due to the rigid backbones of the copolymers that limits the chain motion.[39]

The UV–vis absorption spectra of the copolymer solutions (in *o*-xylene) are shown in Figure S2 (Supporting Information). Both copolymers exhibited somewhat temperature dependent absorption behaviors. From room temperature to 90 °C, both the absorption peak and the absorption onset of PBDT-TDZ exhibited blue-shift of almost 20 nm. In the case of PBDTS-TDZ, the absorption peak blue-shifted 20 nm, while only 10 nm for the absorption onset. In addition, a more obvious absorption peak shoulder could be observed in PBDTS-TDZ solution at room temperature. The results indicated that PBDTS-TDZ with alkylthio side chains had stronger intermolecular interactions than PBDT-TDZ.[17] PBDTS-TDZ also showed a higher maximum absorption coefficient (3.1×10^6 M^{-1} cm^{-1}) than that of PBDT-TDZ (2.5×10^6 M^{-1} cm^{-1}), which would be beneficial for light harvesting in the related OSC devices. Going from solution to film state, both copolymers exhibited the slightly red-shift absorption with more obvious peak shoulders (Figure 1b), implying their further enhanced molecular aggregations. The bandgaps (E_g^{opt}s) were estimated to be 2.07 and 2.09 eV for PBDT-TDZ and PBDTS-TDZ, respectively, which could be comparable to that of P3HT and matched well with the typical low-bandgap acceptor of ITIC (1.58 eV, Figure 1b), thus giving rise to a desirable complementary absorption (Figure S3, Supporting Information).

The energy levels were tested by cyclic voltammetry measurements (Figure S4, Supporting Information; Figure 1c). The HOMO and lowest unoccupied molecular orbital (LUMO) levels were estimated to be –5.35/2.78 and –5.39/–2.79 eV for PBDT-TDZ and PBDTS-TDZ, respectively. The insertion of sulfur atoms in the side chains had less effect on the bandgap but could effectively lower the corresponding energy levels. The smaller HOMO level offset (0.09 eV) between PBDTS-TDZ (HOMO: –5.39 eV) and ITIC (HOMO: –5.48 eV) would be beneficial for obtaining higher V_{oc} with smaller E_{loss} in the related NF-OSCs. The effects of side chains on the molecular geometries and electronic properties were also studied by density functional theory simulations (Figure S5, Supporting Information).[9,40] The calculated HOMO/LUMO levels were –4.93/–2.51 and –5.13/–2.65 eV for PBDT-TDZ and PBDTS-TDZ, respectively, further confirming that introducing sulfur atoms had positive effect on lowering the energy levels.

The photovoltaic properties of copolymers were investigated from their NF-OSCs with an inverted configuration of glass/indium tin oxide (ITO)/ZnO/copolymer:ITIC/MoO_3/Ag. The optimization procedures involved D/A weight ratios, solvents (Table S3, Supporting Information), and film thicknesses (Figure S6 and Table S4, Supporting Information). Furthermore, the devices with a conventional structure of ITO/poly-(3,4-ethylenedioxythiophene):poly-(styrenesulphonicacid) (PEDOT:PSS)/copolymer:ITIC/Ca/Al were also fabricated to make a comparison (Figure S7 and Table S5, Supporting Information). It was interesting that these copolymer blends performed well in a variety of solvents (Table S3, Supporting Information). The best device performance was achieved by using a green solvent of *o*-xylene at the weight ratio of 1:1 (**Figure 2**a and **Table 1**). PBDT-TDZ devices exhibited a high V_{oc} of 1.02 V, J_{sc} of 15.91 mA cm^{-2}, and FF of 58.1%, resulting in a PCE of 9.43%. Owing to the lower-lying HOMO level of PBDTS-TDZ, its devices showed a significantly improved V_{oc} of 1.10 V. Also combining with the higher J_{sc} of 17.78 mA cm^{-2} and FF of 65.4%, PBDTS-TDZ devices generated the better PCE of 12.80%. If adding a small amount of 1-phenylnapthalene (PN) as the additive, PBDT-TDZ devices showed largely enhanced J_{sc} of 17.15 mA cm^{-2} and FF of 67.7%, giving rise to an elevated PCE of 11.72%. On the contrary, PBDTS-TDZ devices displayed a decreased J_{sc} (17.01 mA cm^{-2}) and FF (55.9%) when adding the same additive of PN, resulting in a decreased PCE of 10.26%. This might be mainly caused by the totally different morphology behaviors induced by adding solvent additive (vide infra). The J_{sc} values were confirmed by external quantum efficiency (EQE) measurements (Figure 2b). The fabricated devices exhibited a wide range EQE response from 300 to 800 nm, which could be thankful for the good complementary absorption of the used donor and acceptor materials. The calculated J_{sc} values (J_{cal}s) were determined to be 15.62 and 17.57 mA cm^{-2} from PBDT-TDZ and PBDTS-TDZ devices without any additive, and 16.81 and 16.68 mA cm^{-2} with adding 0.5% PN (Table 1). The results were consistent with those obtained from *J*–*V* measurements. The internal quantum efficiency (IQE) was also measured to investigate the generation and collection efficiency of charge carriers (Figure S8, Supporting Information).[41] As shown in Figure S8 (Supporting Information), the IQEs were almost more than 85% throughout the absorption range for all the fabricated devices. Especially for PBDT-TDZ:ITIC devices with the additive and PBDTS-TDZ:ITIC without any additive, the IQEs reached over 90% from 450 to 750 nm, implying that almost every absorbed photon was converted to a separated pair of charge carriers and almost all photogenerated carriers were collected by the corresponding electrodes. It is exciting that a high PCE of 12.80% can be easily achieved in such a relatively simple fabrication procedure just using one green solvent even without any post-treatment. In addition, the large V_{oc}s over 1.0 V could also be realized from these NF-OSCs based on our TDZ-BDT copolymers, which are

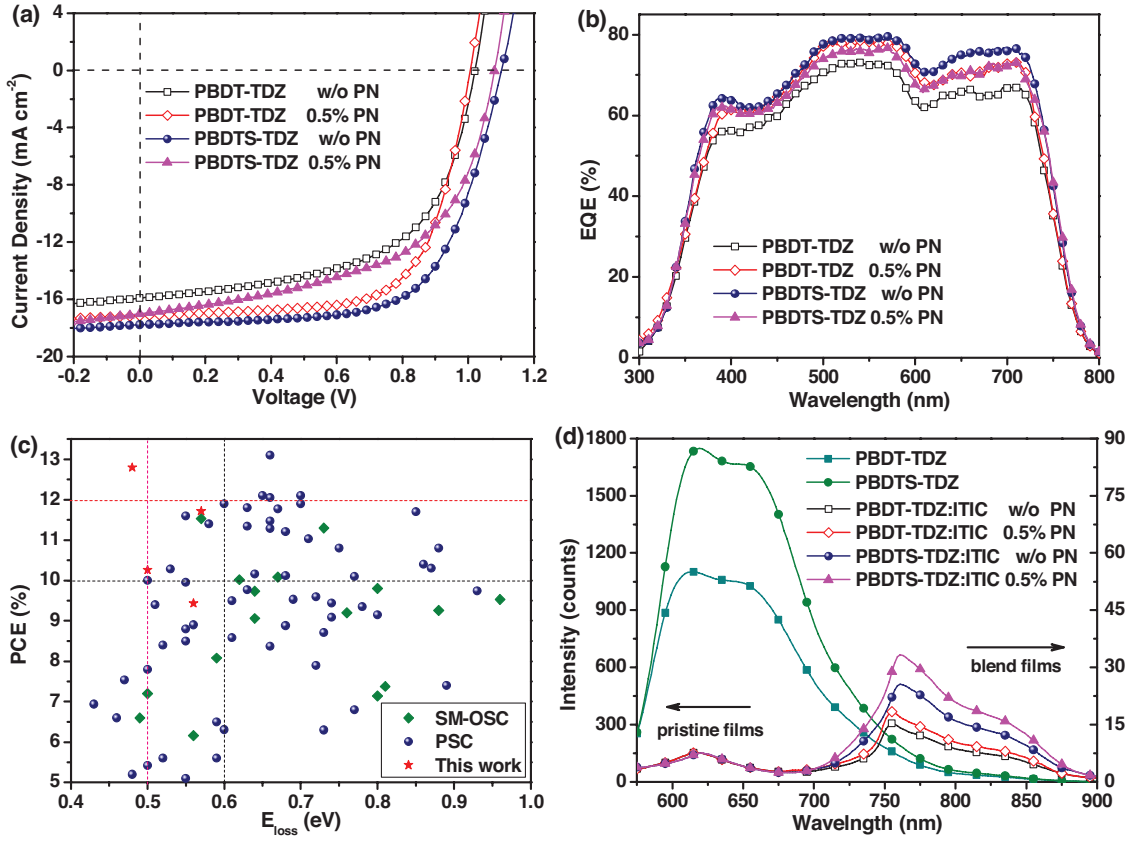

Figure 2. a) *J–V* curves of the nonfullerene organic solar cells. b) EQE curves of the nonfullerene organic solar cells. c) PCE against E_{loss} plots of the reported efficient organic solar cells. d) PL spectra of the pristine and blend films.

among the highest values reported so far (Table S6, Supporting Information). The NF-OSCs in this work showed very low E_{loss} values below 0.6 eV, especially for PBDTS-TDZ devices, which exhibited the lowest value of 0.48 eV. To our best knowledge, this is the best value for any type of OSCs with over 10% PCEs at present (Figure 2c; Table S6, Supporting Information).[14,42] Some reasons should be involved to explain the underlying origins of above low energy loss. First, the small HOMO level offset made the charge transfer state energy (E_{CT}) close to E_g, thus reducing the radiative recombination loss.[17,18] Second, the thiadiazole unit was highly polarizable for increasing the dielectric properties of the resulting copolymers, which could reduce the binding energy of charge transfer excitons. The decreased binding energy not only made the E_{CT} close to E_g but also promoted the charge separation and decreased the charge recombination.[43–45] Finally, high crystallinity and desirable blend morphology of the active layer would also responsible for the efficient charge diffusion and dissociation, leading to decreased nonradiative recombination loss (vide infra).[46–48]

To explore the effect of solvent additive on the devices performance, photoluminescence (PL) spectra of the pristine copolymer and their blend films were detected (Figure 2d). Both copolymers exhibited the strong PL signals in the range of 600–750 nm, which are exactly located in the absorption range of ITIC. The blend films would exhibit noteworthy energy transfer from the copolymer donor to the ITIC acceptor, generating an efficient PL quenching possess. The PL quenching efficiencies were calculated to be 98.6% and 98.7% for PBDT-TDZ and PBDTS-TDZ devices without any additive. However, these values were decreased to 98.3% and 98.1% with adding a small amount of PN. The slightly decreased PL quenching efficiency was originated from the destructive mutual mixing of

Table 1. Device parameters of the nonfullerene organic solar cells.

Active layer	PN	V_{oc} [V]	J_{sc} [mA cm^{-2}]	J_{cal}[a)] [mA cm^{-2}]	FF [%]	PCE_{max}(PCE_{ave})[b)] [%]
PBDT-TDZ:ITIC	w/o	1.02	15.91	15.62	58.1	9.43(9.07 ± 0.36)
	0.5%	1.01	17.15	16.81	67.7	11.72(11.25 ± 0.47)
PBDTS-TDZ:ITIC	w/o	1.10	17.78	17.57	65.4	12.80(12.35 ± 0.45)
	0.5%	1.08	17.01	16.68	55.9	10.26(10.01 ± 0.25)

[a)]The J_{cal} values were determined from the integration of the related EQE curves; [b)]The PCE values in parentheses are average values from at least 20 devices.

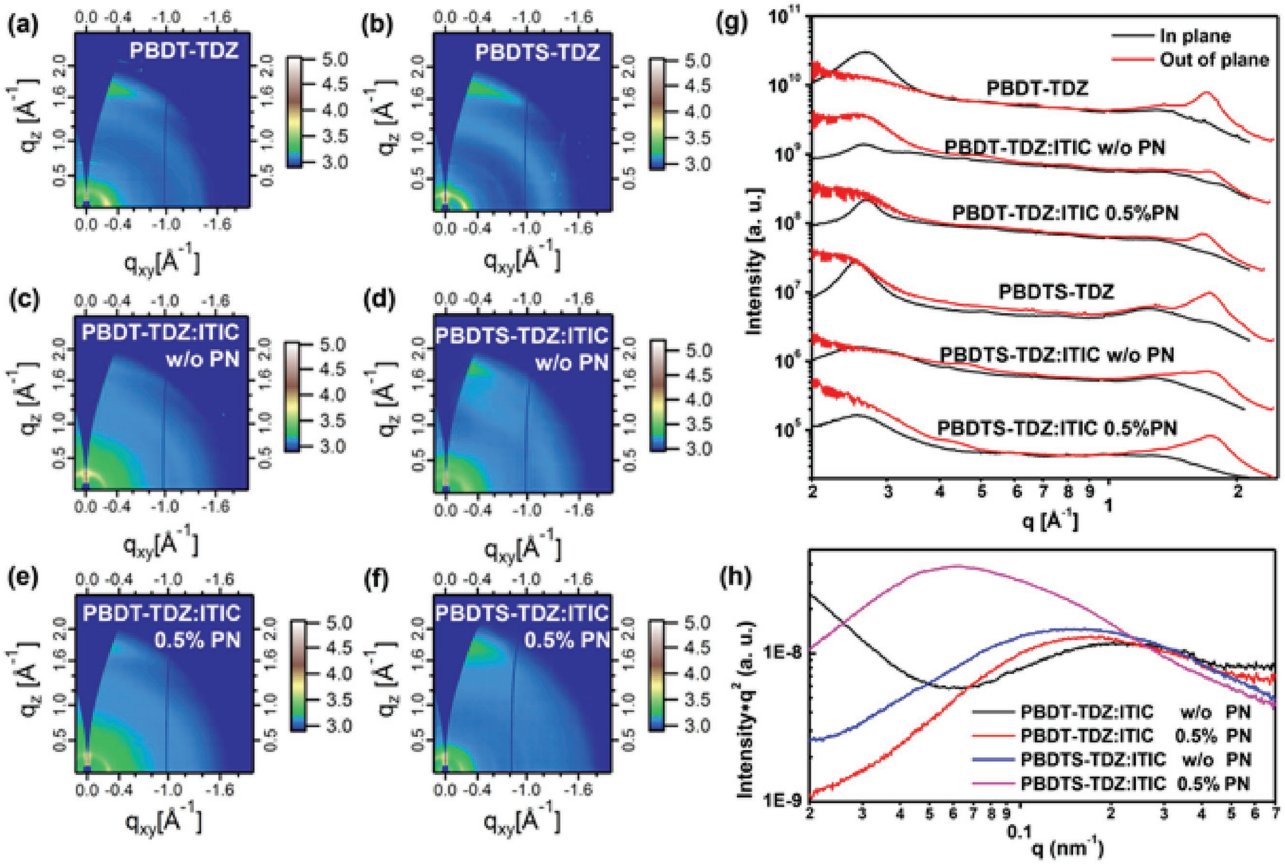

Figure 3. a–f) GIWAXS patterns of the pristine and blend films. g) In-plane and out-of-plane line-cut profiles of the pristine and blend films. h) R-SoXS profiles of the blend films.

the donor and acceptor and serious molecular aggregation with much larger domain sizes.

2D grazing-incidence wide-angle X-ray scattering (2D-GIWAXS) was employed to investigate the microstructure of the neat and blend films (**Figure 3**). Both PBDT-TDZ and PBDTS-TDZ films exhibited two main peaks, showing their crystallinity nature. The (100) peaks in q_{xy} direction were located at 0.27 and 0.25 Å^{-1} for PBDT-TDZ and PBDTS-TDZ, respectively, corresponding to their lamellar stacking distances (d_ls) of 23.3 and 25.1 Å. The larger d_l value of PBDTS-TDZ film came from its relatively longer side chains. But PBDTS-TDZ displayed the stronger (010) peak in the out-of-plane direction, which featured their improved face-on packing behaviors. The π–π tacking distances (d_π) were calculated to be 3.69 and 3.61 Å for PBDT-TDZ and PBDTS-TDZ, respectively. The stronger π–π stacking with a shorter packing distance of PBDTS-TDZ film indicated its better crystallinity, which was induced by the attached alkythio side chains.[17] The crystallinity of both blend films was increased by adding PN as additive. To further analyze the molecular packing behavior, the Herman's orientation parameter of (100) diffraction peak (S_{100}) was calculated for comparison.[49,50] The S_{100} ranges from –0.5 to 1, where –0.5 represents a perfect face-on orientation on the substrate, 1 corresponds to a perfect edge-on orientation and 0 indicates no preferential alignment of the (100) plane.[49,50] The S_{100} values were calculated to be –0.157, 0.053, –0.068 for PBDT-TDZ pure film and PBDT-TDZ:ITIC blends without or with PN as additive, which were also determined to be –0.018, –0.092, –0.078 for the PBDTS-TDZ counterparts. Therefore, the as-cast PBDT-TDZ:ITIC blend exhibited an edge-on packing that would be transferred to face-on orientation after adding the additive. However, the PBDTS-TDZ blends displayed face-on packing property in both conditions, which was decreased by adding the additive. Clearly, the face-on packing would be beneficial for more efficient vertical charge transfer in OSCs. This is one of the reasons why PBDT-TDZ:ITIC devices exhibited lower performance without any additive, while PBDTS-TDZ:ITIC devices showed reduced device performance after adding the additive. In both cases, PBDTS-TDZ:ITIC showed more obvious π–π diffractions than those of PBDT-TDZ:ITIC, implying its higher crystallinity regardless of the processing conditions. The higher crystallinity would be favorable for more efficient charge transport. The hole/electron mobilities of PBDT-TDZ and PBDTS-TDZ blends were determined to be $4.1 \times 10^{-4}/2.3 \times 10^{-4}$ cm^2 V^{-1} s^{-1} and $1.2 \times 10^{-3}/7.2 \times 10^{-4}$ cm^2 V^{-1} s^{-1} without any additive, and $8.5 \times 10^{-4}/6.8 \times 10^{-4}$ cm^2 V^{-1} s^{-1} and $2.1 \times 10^{-3}/6.1 \times 10^{-4}$ cm^2 V^{-1} s^{-1} with adding a small amount of PN (Figure S7, Supporting Information). In contrast to the improved and more balanced hole/electron mobilities of PBDT-TDZ blends treated with PN additive, PBDTS-TDZ blends showed increased hole mobilities but unbalanced hole/electron mobility ratios after adding the same additive. To further verify about this, resonant

soft X-ray scattering (R-SoXS) was performed (Figure 3h). The peaks for PBDT-TDZ:ITIC were located at 0.22 nm^{-1} without the additive and 0.18 nm^{-1} with PN, corresponding to their median domain sizes of 14 and 17 nm on the basis of two-phase separation. When treated with PN additive, the higher domain purity of PBDT-TDZ:ITIC (0.84) with more suitable domain size than the as-cast PBDT-TDZ:ITIC film (0.81) could explain well the improvement of the device performance. However, in the case of PBDTS-TDZ:ITIC, the peaks were located at 0.13 nm^{-1} without any additive and 0.06 nm^{-1} with PN additive, corresponding to their domain sizes of 24 and 52 nm. Although the PN additive significantly improved the domain purity of PBDTS-TDZ:ITIC blend (from 0.86 to 1.0), the generated much larger domain size was definitely detrimental to the charge diffusion and dissociation. The balanced tradeoff between the domain purity and the domain size was in consistence with the best efficiency of the PBDTS-TDZ:ITIC devices without adding any additive.

Atomic force microscopy (AFM) and transmission electron microscopy (TEM) measurements were performed to study the morphology of the active layers. As shown in Figure S10 (Supporting Information), the pristine PBDT-TDZ blend exhibited a rather smooth top surface with the root mean square (RMS) roughness of 0.74 nm. Small grain-like domains were also observed in both AFM and TEM images. But the PN-treated PBDT-TDZ blend appeared a slightly larger RMS value of 1.02 nm with an improved nanophase separation. The interpenetrating fibrils observed in the TEM image were beneficial for effective exciton dissociation and charge transfer, which was consistent with the enhanced J_{sc} and FF values in the corresponding OSC device. On the other side, in the case of PBDTS-TDZ blend, the as-cast film exhibited nicely smooth surface (RMS = 1.10 nm) with desirable small domains and fibril-like networks. However, the RMS was increased to 2.03 nm when adding a small amount of PN additive. The larger aggregations were observed in the AFM and TEM images, which were served as the adverse traps and led to the larger probability of charge recombination in the related OSC devices (Figure S11, Supporting Information). Above observations clearly showed the evolution process of molecular aggregation behavior by adding the PN additive, which could exactly explain the reason why the device performance was improved in PBDT-TDZ devices while reduced in PBDTS-TDZ devices in the presence of PN additive.

Although high PCEs were achieved in single-junction OSCs, the device performances were still limited by the thin film thickness (≈100 nm) and incomplete light harvesting ability (maximum absorption: 0.45, Figure S3, Supporting Information). Fabricating homotandem cells might be a feasible approach to overcome such limitation and further elevate the efficiency of NA-OSCs. Furthermore, the single green solvent processing process in this work would simplify the fabrication procedure of tandem cells, which is helpful for realizing practical applications in the near future. Thus, homotandem cells were tried with a device structure of glass/ITO/ZnO/PBDTS-TDZ:ITIC/PEDOT:PSS/ultrathin Ag/ZnO/PBDTS-TDZ:ITIC/MoO_3/Ag (**Figure 4**). The active layer thickness of the bottom cell was optimized to be 80 nm, while that was changed from 80 to

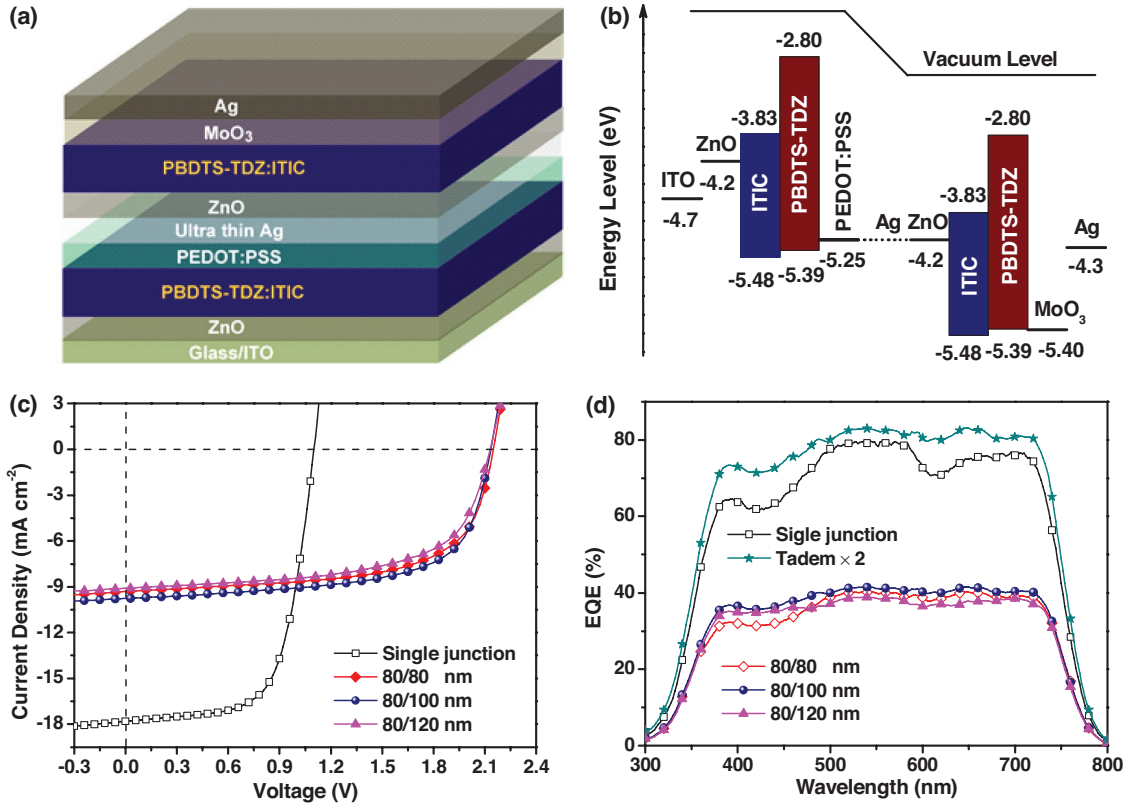

Figure 4. a) Device structure of the homotandem solar cells. b) Energy level diagram representing each layer used in the homotandem architecture. c) *J–V* curves of the homotandem solar cells. d) EQE curves of the homotandem solar cells.

Table 2. Device parameters of the homotandem nonfullerene polymer solar cells.

Film thickness [nm]	V_{oc} [V]	J_{sc} [mA cm^{-2}]	J_{cal}[a)] [mA cm^{-2}]	FF [%]	$PCE_{max}(PCE_{ave})$[b)] [%]
80/80	2.14	9.31	9.12	63.5	12.66(12.20 ± 0.46)[b)]
80/100	2.13	9.77	9.56	64.1	13.35(12.92 ± 0.43)
80/120	2.13	9.10	8.93	61.5	11.92(11.54 ± 0.38)

[a)]The J_{cal} values were determined from the integration of the related EQE curves; [b)]The PCE values in parentheses are average values from at least 20 devices.

120 nm for the top cell (**Table 2**). Finally, the optimal film thickness of the top cell was determined to be 100 nm. The resulting tandem cells exhibited a high V_{oc} of 2.13 V, J_{sc} of 9.77 mA cm^{-2}, and FF of 64.1%, giving rise to the overall PCE of 13.35%. The photovoltaic performance of the best tandem device was certified by the National Photovoltaic Product Quality Supervision & Inspection Center of China and a certified PCE of 13.19% was achieved (Figure S12, Supporting Information). To our best knowledge, this is a new record for homotandem OSCs at present. Beside the largely elevated V_{oc}, the improvement of device performance also came from the enhanced light absorption by the stacked sub-cells, which was further confirmed by EQE measurements (Figure 4b). The EQE of the tandem device here is defined as the ratio of the total converted carriers by the two sub-cells to the sum of the incident photons, which can be estimated by measuring the photoresponse of the tandem cell and then multiplying it by two to represent the total number of photons being converted to electrons.[24] Compared to the single-junction devices, the tandem cells exhibited significantly improved EQE response in the whole absorption range, demonstrating the enhanced light harvesting ability. The successful application of PBDTS-TDZ in homotandem devices gave a good example for developing high-performance NF-OSCs.

In summary, two novel wide-bandgap copolymers, PBDT-TDZ and PBDTS-TDZ, were designed and synthesized for efficient single-junction OSCs and homotandem solar cells. The newly developed copolymers exhibited a wide bandgap up to 2.10 eV and low-lying HOMO levels below −5.35 eV. Using ITIC as the nonfullerene acceptor, the resulting single-junction devices based on PBDTS-TDZ exhibited a high V_{oc} of 1.10 V and a small E_{loss} of 0.48 eV. The extremely small HOMO offset of 0.09 eV between PBDTS-TDZ and ITIC caused by the introduced alkylthio side chains had less effect on the exciton dissociation process. Compared to PBDT-TDZ devices, the PBDTS-TDZ devices exhibited a high PCE of 12.80% just processing with a single green solvent of *o*-xylene but without any post-treatment. When employing a homotandem structure, the tandem cells based on PBDTS-TDZ showed the significantly elevated PCE of 13.35% with a very high V_{oc} of 2.13 V. This work provides a new insight in developing high-performance wide-bandgap copolymer donors for single-junction and tandem NF-OSCs.

Supporting Information

Supporting Information is available from the Wiley Online Library or from the author.

Acknowledgements

This work was supported by the NSFC (Grant Nos. 51573107, 91633301, and 21432005) and the Foundation of State Key Laboratory of Polymer Materials Engineering (sklpme2017-2-04).

Conflict of Interest

The authors declare no conflict of interest.

Keywords

1,3,4-thiadiazole, green solvent, homotandem solar cells, nonfullerene organic solar cells, wide-bandgap copolymers

Received: July 17, 2017
Revised: September 23, 2017
Published online: December 6, 2017

[1] Y. F. Li, *Acc. Chem. Res.* **2012**, *45*, 723.
[2] L. T. Dou, Y. S. Liu, Z. R. Hong, G. Li, Y. Yang, *Chem. Rev.* **2015**, *115*, 12633.
[3] H. F. Yao, L. Ye, H. Zhang, S. S. Li, S. Q. Zhang, J. H. Hou, *Chem. Rev.* **2016**, *116*, 7397.
[4] B. C. Thompson, J. M. J. Fréchet, *Angew. Chem., Int. Ed.* **2008**, *47*, 58.
[5] J. B. Zhao, Y. K. Li, G. F. Yang, K. Jiang, H. R. Lin, H. Ade, W. Ma, H. Yan, *Nat. Energy* **2016**, *1*, 15027.
[6] Y. W. Duan, X. P. Xu, H. Yan, W. L. Wu, Z. J. Li, Q. Peng, *Adv. Mater.* **2017**, *29*, 1605115.
[7] G. J. Zhang, G. F. Yang, H. Yan, J. H. Kim, H. Ade, W. L. Wu, X. P. Xu, Y. W. Duan, Q. Peng, *Adv. Mater.* **2017**, *29*, 1606054.
[8] C. B. Nielsen, S. Holliday, H. Y. Chen, S. J. Cryer, I. McCulloch, *Acc. Chem. Res.* **2015**, *48*, 2803.
[9] W. C. Zhao, S. S. Li, H. F. Yao, S. Q. Zhang, Y. Zhang, B. Yang, J. H. Hou, *J. Am. Chem. Soc.* **2017**, *139*, 7148.
[10] Y. Cui, H. F. Yao, B. W. Gao, Y. P. Qin, S. Q. Zhang, B. Yang, C. He, B. W. Xu, J. H. Hou, *J. Am. Chem. Soc.* **2017**, *139*, 7302.
[11] T. Yu, X. P. Xu, G. Zhang, J. H. Wan, Y. Li, Q. Peng, *Adv. Funct. Mater.* **2017**, *27*, 1701491.
[12] Y. Z. Lin, Z. G. Zhang, H. T. Bai, J. Y. Wang, Y. H. Yao, Y. F. Li, D. B. Zhu, X. W. Zhan, *Energy Environ. Sci.* **2015**, *8*, 610.
[13] Y. Z. Lin, J. Y. Wang, Z. G. Zhang, H. T. Bai, Y. F. Li, D. B. Zhu, X. W. Zhan, *Adv. Mater.* **2015**, *27*, 1170.
[14] S. S. Li, L. Ye, W. C. Zhao, S. Q. Zhang, S. Mukherjee, H. Ade, J. H. Hou, *Adv. Mater.* **2016**, *28*, 9423.
[15] F. W. Zhao, S. X. Dai, Y. Wu, Q. Q. Zhang, J. Y. Wang, L. Jiang, Q. D. Ling, Z. X. Wei, W. Ma, W. You, C. R. Wang, X. W. Zhan, *Adv. Mater.* **2017**, *29*, 1700144.
[16] S. S. Chen, Y. H. Liu, L. Zhang, P. C. Y. Chow, Z. Wang, G. Y. Zhang, W. Ma, H. Yan, *J. Am. Chem. Soc.* **2017**, *139*, 6298.
[17] J. H. Wan, X. P. Xu, G. J. Zhang, Y. Li, K. Feng, Q. Peng, *Energy Environ. Sci.* **2017**, *10*, 1739.
[18] J. Liu, S. S. Chen, D. P. Qian, B. Gautam, G. F. Yang, J. B. Zhao, J. Bergqvist, F. L. Zhang, W. Ma, H. Ade, O. Inganäs, K. Gundogdu, F. Gao, H. Yan, *Nat. Energy* **2016**, *1*, 16089.
[19] L. Y. Lu, T. Y. Zheng, Q. H. Wu, A. M. Schneider, D. L. Zhao, L. P. Yu, *Chem. Rev.* **2015**, *115*, 12666.
[20] L. Ye, W. C. Zhao, S. S. Li, S. Mukherjee, J. H. Carpenter, O. Awartani, X. C. Jiao, J. H. Hou, H. Ade, *Adv. Energy Mater.* **2017**, *7*, 1602000.

[21] Y. H. Liu, J. B. Zhao, Z. K. Li, C. Mu, W. Ma, H. W. Hu, K. Jiang, H. R. Lin, H. Ade, H. Yan, *Nat. Commun.* **2014**, *5*, 5293.
[22] S. Holliday, R. S. Ashraf, A. Wadsworth, D. Baran, S. A. Yousaf, C. B. Nielsen, C. H. Tan, S. D. Dimitrov, Z. Shang, N. Gasparini, M. Alamoudi, F. Laquai, C. J. Brabec, A. Salleo, J. R. Durrant, I. McCulloch, *Nat. Commun.* **2016**, *7*, 11585.
[23] M. M. Li, F. Liu, X. J. Wan, W. Ni, B. Kan, H. R. Feng, Q. Zhang, X. Yang, Y. C. Wang, Y. M. Zhang, Y. Shen, T. P. Russell, Y. S. Chen, *Adv. Mater.* **2015**, *27*, 6296.
[24] S. Q. Zhang, L. Ye, H. Zhang, J. H. Hou, *Mater. Today* **2016**, *19*, 533.
[25] H. Zhang, H. F. Yao, W. C. Zhao, L. Ye, J. H. Hou, *Adv. Energy Mater.* **2016**, *6*, 1502177.
[26] S. S. Chen, G. Y. Zhang, J. Liu, H. T. Yao, J. Q. Zhang, T. X. Ma, Z. K. Li, H. Yan, *Adv. Mater.* **2017**, *29*, 1604231.
[27] J. B. You, C. C. Chen, Z. R. Hong, K. Yoshimura, K. Ohya, R. Xu, S. L. Ye, J. Gao, G. Li, Y. Yang, *Adv. Mater.* **2013**, *25*, 3973.
[28] H. Zhou, Y. Zhang, C. K. Mai, S. D. Collins, G. C. Bazan, T. Q. Nguyen, A. J. Heeger, *Adv. Mater.* **2015**, *27*, 1767.
[29] Y. J. Li, J. K. Geng, Y. Liu, S. H. Yu, G. S. Zhao, *ChemMedChem* **2013**, *8*, 27.
[30] W. N. Wu, A. Q. Tai, Q. Chen, G. P. Ouyang, *J. Heterocycl. Chem.* **2016**, *53*, 626.
[31] N. S. El-Gohary, M. I. Shaaban, *Arch. Pharm. Chem. Life Sci.* **2015**, *348*, 283.
[32] A. G. Gadhave, R. B. Gaikar, S. R. Kuchekar, B. K. Karale, *J. Heterocycl. Chem.* **2014**, *51*, 1849.
[33] T. Umeyama, E. Douvogianni, H. Imahori, *Chem. Lett.* **2012**, *41*, 354.
[34] T. Higashihara, H. C. Wu, T. Mizobe, C. Lu, M. Ueda, W. C. Chen, *Macromolecules* **2012**, *45*, 9046.
[35] T. Higashihara, T. Mizobe, C. Lu, W. C. Chen, M. Ueda, *J. Photopolym. Sci. Technol.* **2013**, *26*, 185.
[36] S. Fukuta, Z. Wang, S. Miyane, T. Koganezawa, T. Sano, J. Kido, H. Mori, M. Ueda, T. Higashihara, *Polym. J.* **2015**, *47*, 513.
[37] S. Fukuta, J. Seo, H. Lee, H. Kim, Y. Kim, M. Ree, T. Higashihara, *Macromolecules* **2017**, *50*, 891.
[38] C. Weng, L. Gao, Z. Zhang, Z. Liu, S. Tan, Y. Li, *J. Polym. Sci., Part B: Polym. Phys.* **2017**, *55*, 990.
[39] I. Osaka, M. Shimawaki, H. Mori, I. Doi, E. Miyazaki, T. Koganezawa, K. Takimiya, *J. Am. Chem. Soc.* **2012**, *134*, 3498.
[40] X. P. Xu, K. Feng, K. Li, Q. Peng, *J. Mater. Chem. A* **2015**, *3*, 23149.
[41] Y. X. Li, L. Zhong, B. Gautam, H. J. Bin, J. D. Lin, F. P. Wu, Z. J. Zhang, Z. Q. Jiang, Z. G. Zhang, K. Gundogdu, Y. F. Li, L. S. Liao, *Energy Environ. Sci.* **2017**, *10*, 1610.
[42] S. H. Park, A. Roy, S. Beaupre, S. Cho, N. Coates, J. S. Moon, D. Moses, M. Leclerc, K. Lee, A. J. Heeger, *Nat. Photonics* **2009**, *3*, 297.
[43] B. Carsten, J. M. Szarko, H. J. Son, W. Wang, L. Lu, F. He, B. S. Rolczynsk, S. J. Lou, L.X. Chen, L. P. Yu, *J. Am. Chem. Soc.* **2011**, *133*, 20468.
[44] C. J. Takacs, Y. M. Sun, G. C. Welch, L. A. Perez, X. F. Liu, W. Wen, G. C. Bazan, A. J. Heeger, *J. Am. Chem. Soc.* **2012**, *134*, 16597.
[45] J. J. Intemann, K. Yao, F. Z. Ding, Y. X. Xu, X. K. Xin, X. S. Li, A. K.-Y. Jen, *Adv. Funct. Mater.* **2015**, *25*, 4889.
[46] T. M. Burke, S. Sweetnam, K. Vandewal, M. D. McGehee, *Adv. Energy Mater.* **2015**, *5*, 1500123.
[47] T. Heumueller, T. M. Burke, W. R. Mateker, I. T. Sachs-Quintana, K. Vandewal, C. J. Brabec, M. D. McGehee, *Adv. Energy Mater.* **2015**, *5*, 1500111.
[48] S. D. Collins, C. M. Proctor, N. A. Ran, T. Q. Nguyen, *Adv. Energy Mater.* **2016**, *6*, 1501721.
[49] L. A. Perez, P. Zalar, L. Ying, K. Schmidt, M. F. Toney, T. Q. Nguyen, G. C. Bazan, E. J. Kramer, *Macromolecules* **2014**, *47*, 1403.
[50] A. M. Hiszpanski, S. S. Lee, H. Wang, A. R. Woll, C. Nuckolls, Y. L. Loo, *ACS Nano* **2013**, *7*, 294.

